Full Length Article

Sooting propensity of dimethyl carbonate, soot reactivity and characterization

Katiuska Alexandrino

Juan Salinas

Ángela Millera

Rafael Bilbao

María U. Alzueta*

uxue@unizar.es

Aragón Institute of Engineering Research (I3A), Department of Chemical and Environmental Engineering, University of Zaragoza, C/ Mariano Esquillor, s/n, 50018 Zaragoza, Spain

*Corresponding author.

Abstract

Oxygenated compounds have gained interest in the last few years because they represent an attractive alternative as additive to diesel fuel for reducing soot emissions. Although dimethyl carbonate (DMC) seems to be a good option, studies about its propensity to form soot, as well as the knowledge of the characteristics of this soot are still missing. For that reason, this paper focuses on the potential of DMC to form soot, as well as on the reactivity and characterization of this soot. Results from pyrolysis experiments performed in an atmospheric pressure flow reactor at different temperatures (1075–1475 K) and inlet DMC concentrations (approximately 33,333 and 50,000 ppm) show that both soot and gas yields are affected by the pyrolysis temperature, while an increase in the inlet DMC concentration only affects slightly the soot yield, without notable influence on the gas yield. DMC shows a very low tendency to produce soot because the CO/CO_2 formation is favoured and thus few carbon atoms are available for soot formation. A chemical kinetic model developed, without incorporating soot particles dynamics, can predict well the gas-phase trends. The comparison of the soot amount profile obtained with the PAH amount profile determined by the model suggests a good first approach toward a model including soot formation. The soot reactivity study toward O_2 (500 ppm) and NO (2000 ppm) at 1475 K, as well as its characterization, show that the higher the temperature and the inlet DMC concentration of soot formation, the lower the reactivity of the soot.

Keywords: Dimethyl carbonate; Pyrolysis; Soot; Reactivity; Characterization

1 Introduction

Dimethyl carbonate (DMC, $CH_3OCOOCH_3$), a carbonate ester ~~also called methylal~~, is an attractive oxygenate compound for using as diesel fuel component for reducing soot emissions due to its good characteristics, such as: (1) 100% miscibility in diesel; (2) 53 wt% in oxygen content; (3) no carbon–carbon atomic bonds; and (4) relatively high H/C ratio [1,2].

Diesel-DMC blends have been tested in diesel engines showing potential to reduce smoke and soot emissions (e.g. [1]). Furthermore, when comparing with diesel and biodiesel emissions, adding DMC to diesel showed the capacity to reduce unregulated carcinogenic emissions, such as benzene and 1,3-butadiene [2].

Previous studies have contributed to the knowledge of the DMC decomposition and the DMC combustion (e.g. [3–5]). Kinetic studies on DMC conversion are also reported in literature [5–7]. However, experimental data on sooting tendency of DMC complemented with computations based on detailed chemical kinetic mechanisms, and furthermore reactivity and characterization studies of the soot obtained from the DMC conversion, are still missing. The determination of the potential of DMC to form soot is important to establish practical conclusions on how the addition of DMC to diesel fuel affects the sooting tendency of fuel mixtures. Furthermore, knowledge of the soot reactivity is important to develop soot reduction strategies. Therefore, the main goals of the present work are to perform the DMC pyrolysis in a wide range of temperature (1075–1475 K) and with different inlet DMC concentrations (33,333 and 50,000 ppm, corresponding to 100,000 and 150,000 ppm of inlet total carbon amount, respectively) in order to study the ability of

DMC to form soot under different pyrolytic conditions, and to compare the experimental data with the results of a detailed gas-phase chemical kinetic model, which involves the formation of species known to be involved in the soot formation process. Additionally, the reactivity study of soot samples toward different gases present in the combustion chamber of a diesel engine, such as O_2 and NO, is carried out, as well as the characterization of soot samples using several instrumental techniques (elemental analysis, determination of the BET surface area with N_2 at 77 K, scanning electron microscopy (SEM), transmission electron microscopy (TEM), X-ray diffraction (XRD), and Raman spectroscopy), in order to evaluate their composition and structural properties, and relate them to their reactivity.

2 Experimental procedure and set-up

The atmospheric thermal decomposition of DMC was carried out varying the reaction temperature (1075, 1175, 1275, 1325, 1375, 1425, and 1475 K) for each inlet DMC concentration studied (approximately 33,333 and 50,000 ppm). The experimental facility used was described elsewhere (e.g. [8]) and is briefly reiterated here. Reaction takes place within a quartz tube reactor of 45 mm internal diameter and 800 mm length situated inside an electric furnace. The reactor inlet and outlet are air-cooled without direct contact with the reaction mixture, and resulting in an isothermal reaction zone length of 160 mm, with a flat temperature profile ±25 K. The longitudinal temperature profile inside the reactor is measured with an S-type thermocouple at a total N_2 flow rate of 1000 mL (STP)/min with an estimated uncertainty of ±5. Example of temperature profiles for 1475, 1375, and 1275 K are provided in the supplementary material (Fig. S1). DMC is fed into the reactor in gas-phase using an isocratic HPLC pump, a thermally isolated line, and N_2 as carrier gas. N_2 is added into the reactor to obtain a total gas flow rate of 1000 mL (STP)/min, resulting in a gas residence time in the reaction zone dependent on temperature, $t_r = 4168/T(K)$ (s) (t_r = 2.83–3.88 s, in the temperature range studied).

The reactor outlet is linked to a soot collection system consisting of a quartz fiber filter with a pore diameter lower than 1 μm, and a light gases measurement system consisting of a gas chromatograph (GC) (Agilent 6890A) (accuracy of ±10 ppm), which is calibrated to quantify: methane, methanol, ethylene, acetylene, ethane, dimethyl ether, propadiene, propylene, propane, 1,3-butadiene, benzene, ethylbenzene, toluene, CO, CO_2, and H_2. The total time for each experiment was fixed in 3 h, not exceeding an overpressure limit of 1.3 bar inside the reactor in order to avoid perturbations in the experimental set-up.

Reactivity experiments were carried out using the facility and following the steps described in previous works [8,9]. Briefly, the reaction takes place within a quartz tubular reactor which has a bottleneck in the middle in which a quartz wool plug is introduced to locate the soot/silica sand mixture (i.e., 10 mg of soot mixed with 300 mg of silica sand (150–300 μm) to prevent soot particle agglomeration and to be able to consider isolated particles), resulting in a thin layer. The reactor is located in an electrical furnace which is heated to the reaction temperature (1275 K) at 10 K/min in a N_2 atmosphere (1000 mL (STP)/min). Once the reaction temperature desired is reached, part of the N_2 flow is replaced by the flow of the reactant gas, O_2 or NO, to attain a concentration of 500 ppm of O_2 or 2000 ppm of NO in the total flow rate of 1000 mL (STP)/min. These O_2 and NO concentrations were selected to be consistent with previous experiments [8,9]. The gas products are air-cooled down to room temperature and measured by continuous CO/CO_2 and NO ABB infrared analyzers, which provide uncertainty measurements below 5%.

Selected soot samples were characterized by different instrumental techniques, namely: elemental analysis, determination of the BET surface area with N_2 at 77 K, scanning electron microscopy (SEM), transmission electron microscopy (TEM), X-ray diffraction (XRD), and Raman spectroscopy.

Before performing both soot reactivity experiments and soot characterization, the soot samples were undergone to a thermal annealing during 1 h in a N_2 atmosphere at their formation temperature in order to eliminate the adsorbed compounds [8].

3 Kinetic model

The chemical reaction mechanism used for the simulations of the experimental results was built based on Alzueta et al. [7] mechanism, which implements the DMC conversion sub-mechanism by Glaude et al. [6]. With the aim of improving model predictions under sooting conditions, reactions involving benzene, toluene, and other intermediates such as phenyl radicals [10] were added to the base mechanism [7]. Also, the mechanism was extended to include different pathways for the polycyclic aromatic hydrocarbon (PAH) formation, which are generally accepted to be the responsible molecules for the soot particle inception stage [11,12], specifically: (1) H-abstraction/C_2H_2-addition (HACA) (starting with the C_2H_2 addition to phenyl radical); (2) the combination of phenyl radicals with benzene; (3) the cyclopentadienyl radicals recombination; and (4) the combination of benzyl and propargyl radicals. The HACA mechanism occurs through a two-step repeating sequence involving hydrogen abstraction to activate aromatics, followed by subsequent acetylene addition. This process continues leading to the sequential formation of multi-ring structures [13]. The rate constants proposed by Appel et al. [11] for PAH growth up to pyrene and the rate constants for the PAH growth from pyrene up to coronene proposed by Richter et al. [12] were used. Mechanism for the PAH oxidation by Appel et al. [11] was also added. In this way, the kinetic model only includes gas-phase chemistry and does not include soot particle dynamics. However, this gas-phase model could be a first approach toward a complete model including soot formation.

The modified gas-phase reaction mechanism consists of 262 chemical species and 1182 reactions (It can be found in the supplementary material). All model computations were conducted with the SENKIN

code of the Chemkin software package [14].

4 Results and discussion

Fig. 1 presents the soot and gas yields (in percentage), as a function of temperature, obtained during the pyrolysis of different inlet DMC concentrations. Both soot and gas yields are defined as the carbon amount in soot and gases, respectively, related to the total carbon amount at the reactor inlet [9]. It is worth to clarify that the gas yield includes the DMC amount that did not react and was found at the reactor outlet. It can be observed that, for both inlet DMC concentrations, soot appears to be formed from 1375 K, reaching a maximum soot yield value of approximately 9 and 12% at 1475 K, for $[DMC]_{inlet}$ = 33,333 and 50,000 ppm, respectively. The rise of temperature causes both an increase in soot yield and a decrease in gas yield for the two inlet DMC concentrations evaluated. This is consistent with previous findings [8,9]. An increase in the DMC concentration only affects slightly the soot yield, without notable influence on the gas yield.

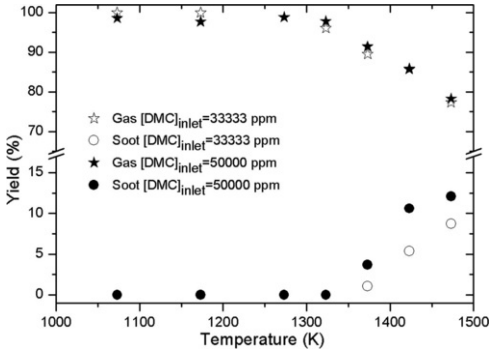

Fig. 1 Soot and gas yields, as a function of temperature, obtained in the DMC pyrolysis of 33,333 and 50,000 ppm from 1075 to 1475 K.

Fig. 2 shows the DMC conversion (X_{DMC}) as a function of temperature for the two inlet DMC concentrations used, as well as the measured (symbols) and predicted (lines) major gases concentration profiles (ethylene, acetylene, H_2, benzene, methane, CO, and CO_2). Other gases (not shown), such as methanol and dimethyl ether at 1075 K, and ethane at 1075, 1175 and 1275 K were detected with low concentrations. Overall, modelling trends are consistent with the experimental data trends. The experimental results indicate a high DMC conversion (≥89%) throughout the temperature range studied, obtaining a slight increase in the conversion for the lowest inlet DMC concentration, while model calculations show a conversion of 100% for both inlet DMC concentrations. According to model calculations, most of DMC can be consumed either by decomposition or by reaction with H radicals. By decomposition, DMC yields CO_2 via CH_3OCOO radicals (reactions R1 and R2), or yields CO via methoxy radicals (CH_3O) (reactions R1–R5). By reaction with H radicals, DMC yields the so-called DMC radical ($CH_3OCOOCH_2$), which in turn decomposes into methoxy formyl radicals (CH_3OCO) forming lastly CO_2 (reactions R6–R8).

$$CH_3OCOOCH_3 \rightleftarrows CH_3OCOO + CH_3 \quad \textbf{(R1)}$$

$$CH_3OCOO \rightleftarrows CH_3O + \mathbf{CO_2} \quad \textbf{(R2)}$$

$$CH_3O(+M) \rightleftarrows CH_2O + H(+M) \quad \textbf{(R3)}$$

$$CH_2O + H \rightleftarrows HCO + H_2 \quad \textbf{(R4)}$$

$$HCO + M \rightleftarrows H + \mathbf{CO} + M \quad \textbf{(R5)}$$

$$CH_3OCOOCH_3 + H \rightleftarrows CH_3OCOOCH_2 + H_2 \quad \textbf{(R6)}$$

$$CH_3OCOOCH_2 \rightleftarrows CH_3OCO + CH_2O \quad \textbf{(R7)}$$

$$CH_3OCO \rightleftarrows CH_3 + \mathbf{CO_2} \quad \textbf{(R8)}$$

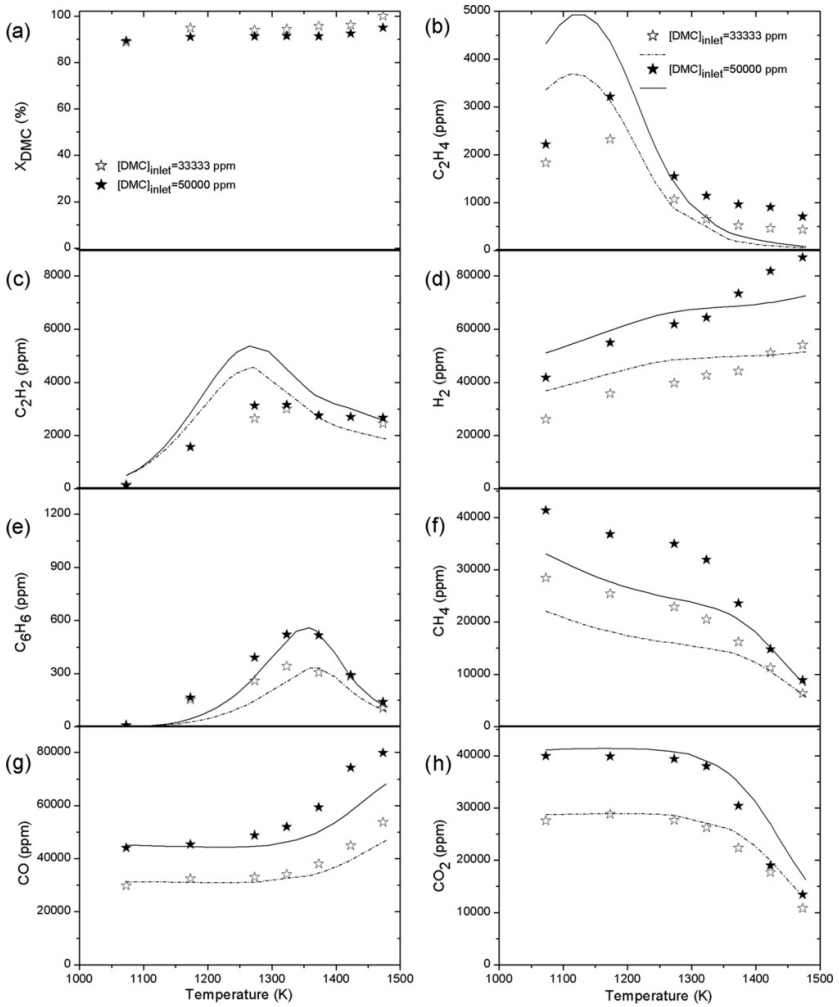

Fig. 2 (a) DMC conversion, and (b)–(h) measured (symbols) and predicted (lines) concentration profiles of the major gases analyzed in the DMC pyrolysis.

Ethylene concentration exhibits a maximum around 1075–1175 K (Fig. 2b). Its consumption is to yield acetylene via reaction with vinyl radicals (C_2H_3), and by direct decomposition. Fig. 2c shows that experimental acetylene concentration achieves a maximum around 1325–1375 K, while calculations slightly shift this maximum toward lower temperatures (around 1265 K). The experimental matching of the temperature at which the maximum acetylene concentration is achieved, and the temperature at which soot begins to be formed (1375 K, in Fig. 1), suggests that probably acetylene is consumed to yield PAH through the HACA mechanism.

It is observed in Fig. 2d that an increase in temperature leads to an increase in H_2 concentration, which is released during the PAH growth through the HACA mechanism. Experimentally, the increase of hydrogen formation is more pronounced at 1375 K, which fits with the soot formation temperature (Fig. 1). Regarding to benzene, its concentration profile (Fig. 2e) shows a maximum around 1325–1375 K and its consumption is involved in a reaction sequence producing species that yield soot.

Fig. 2f shows that the CH_4 concentration decreases throughout the temperature range studied. This decrease in CH_4 concentration, which is sharper from 1375 K (the soot formation temperature, Fig. 1), suggests that methyl radicals (CH_3) are involved at high temperatures in the reaction pathways leading to soot formation; while at low temperatures, the methyl radicals formed are recycled back to CH_4 by reaction

with H_2.

Measured and predicted CO and CO_2 concentration profiles, Fig. 2g and h respectively, remain basically constant with the increase of temperature in the 1075–1325 K temperature range. However, from 1375 K, the CO and CO_2 formation is favoured and disfavoured, respectively, as the temperature rises. These trends are opposite to that found in previous works on the pyrolysis of other oxygenates [9,15]. In those works, the CO concentration increases with increasing temperature to subsequently remain constant, while the CO_2 concentration increases monotonically due to the CO + OH $\rightleftarrows$ CO_2 + H reaction, which is favoured at high temperatures. These opposite behaviors can be due to the specific DMC structure. As mentioned above, model calculations indicate that DMC consumption involves the formation of CH_3OCOO and CH_3OCO radicals, which favours the direct CO_2 formation from DMC. This increment in CO_2 concentration in the reaction environment makes the CO + OH $\rightleftarrows$ CO_2 + H reaction to proceed in the reverse sense, increasing the CO concentration, in particular at high temperatures [16].

Because the model does not include the particle mass growth process, which is known to occur via the addition of gas species such as PAH to the nascent soot particles [12], Fig. 3 compares the experimental soot amount collected with the sum of the PAH amount (up to coronene) predicted with the model to help to qualitatively analyze the experimental results. As seen, total PAH amount predicted by model matches well the soot amount collected experimentally. In this way, the present model can be a good first approach toward a complete model including soot formation.

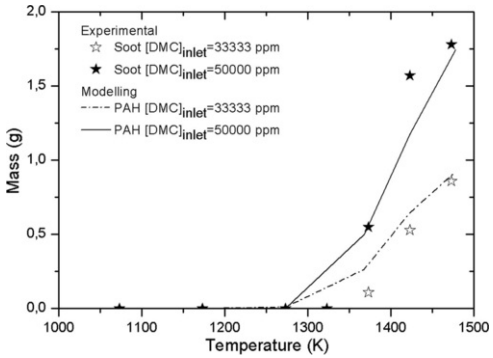

Fig. 3 Comparison of the soot amount collected experimentally with the sum of the PAH amount calculated by modelling.

In order to gain a deeper insight into the low capacity of DMC to form soot, Fig. 4 compares the soot yields obtained in the DMC (33,333 ppm), ethanol (EtOH) (50,000 ppm) [9], and acetylene (50,000 ppm) [17] pyrolysis, in the 1275–1475 K temperature range. These results correspond to an inlet total carbon amount of 100,000 ppm. The acetylene pyrolysis is performed at the same residence times that the DMC pyrolysis, $t_r = 4168/T(K)$ (s), and the EtOH pyrolysis at lower residence times (1.06–1.23 s). As expected, the soot yield in the DMC pyrolysis is much lower than the soot yield in the acetylene pyrolysis, but also DMC has a much lower tendency to form soot than ethanol, even when ethanol pyrolysis is performed at a lower residence time (lower residence times produce less soot [18]). This low propensity of DMC to form soot is due most likely to its structure and reaction mechanism. Unlike DMC, EtOH has carbon-carbon bonds which favours its conversion into ethylene which leads to the acetylene formation and consequently to soot. Nevertheless, DMC is mainly decomposed into CH_3OCOO and CH_3OCO radicals, limiting the soot formation precursors by favouring the CO/CO_2 formation (reactions R1–R8). Also, the decrease in soot formation by DMC may be due to the reduced benzene formation observed during its pyrolysis. In this way, a comparison of the concentration of principal soot precursors (acetylene and benzene) formed in the DMC and EtOH pyrolysis is shown in Fig. 5a and b. It is clear that EtOH has a greater tendency to form acetylene and benzene than DMC. Besides this, DMC has great tendency to form CO and CO_2 (Fig. 5c and d) reducing the levels of carbon atoms available for soot formation.

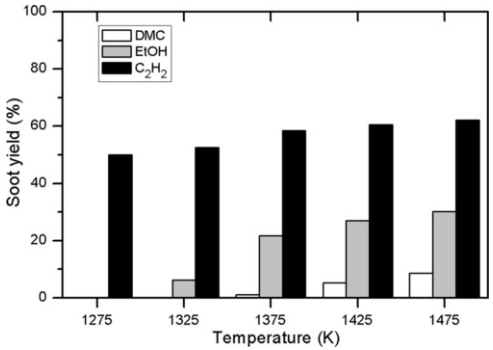

Fig. 4 Comparison of soot yield obtained in the DMC, EtOH [9], and acetylene [17] pyrolysis from 1275 to 1475 K.

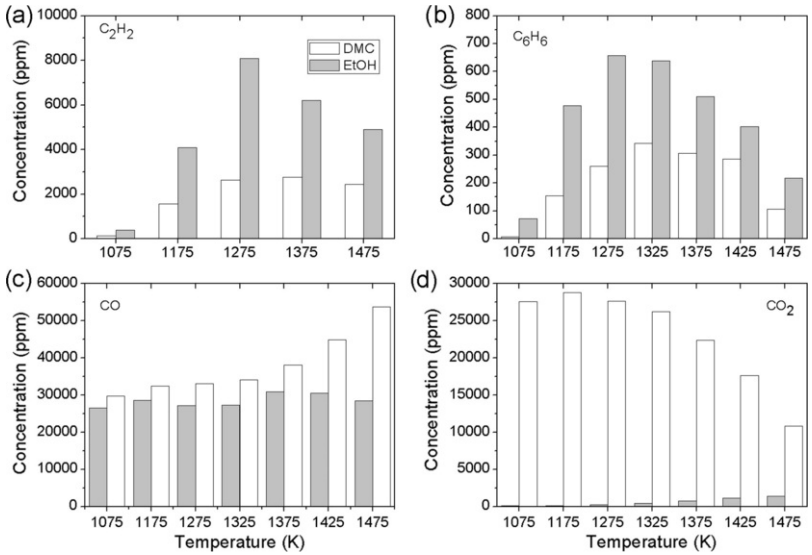

Fig. 5 Comparison of the concentration of (a) acetylene, (b) benzene, (c) CO, and (d) CO_2 measured in the DMC and EtOH pyrolysis [9] from 1075 to 1475 K.

Selected annealed soot samples (obtained with $[DMC]_{inlet}$ = 33,333 ppm at 1425 and 1475 K (DMC3_1425 and DMC3_1475, respectively), and with $[DMC]_{inlet}$ = 50,000 ppm at 1425 and 1475 K (DMC5_1425 and DMC5_1475, respectively)) were subjected to the soot reactivity study.Soot reactivity is analyzed through the carbon conversion (X_c), which is defined as the carbon weight reacted at any time related to the carbon weight fed into the reactor (W_{c_0}):

$$X_c = \frac{(W_{c_0} - W_c)}{W_{c_0}} \quad \textbf{(1)}$$

Being W_c the remaining carbon weight within the reactor at a given time.

During the soot-O_2 and soot-NO interactions, carbon is mainly released from the particles in the form of CO and CO_2 as reaction products. Thereby, W_{c_0} , in mg, is calculated as:

$$W_{c_0} = 10^{-3} M_c F_T \int_0^{\infty} (C_{CO} + C_{CO_2}) dt \quad \textbf{(2)}$$

~~Where~~ where M_c is the carbon atomic weight (g/mol), C_{CO} and C_{CO_2} are the CO and CO_2 concentrations (ppm) at the reactor outlet, respectively, and F_T is the outlet flow (mol/s) given by:

$$F_T = \frac{QP}{R_g T} \quad (3)$$

~~Where~~ where Q is the feeding flow rate (m^3/s), P is the reactor pressure (Pa), R_g is the universal gas constant (Pa m^3/mol K), and T is the reactor temperature (K).

On the other hand, W_c, in mg, can be calculated as:

$$W_c = W_{c_0} - 10^{-3} M_c F_T \int_0^t (C_{CO} + C_{CO_2}) dt \quad (4)$$

Fig. 6 shows the evolution of carbon conversion (X_c) with time for the soot-O_2 and soot-NO interactions. The soot samples are more reactive toward O_2 (Fig. 6a) compared to NO (Fig. 6b), even for a lower O_2 concentration. For a given soot formation temperature, soot formed with the lowest inlet DMC concentration is more reactive toward both O_2 and NO than the soot formed with the highest DMC concentration, and the difference in reactivity is higher at the lower formation temperature. For a given inlet DMC concentration, soot formed at 1425 K is more reactive than the soot formed at 1475 K.A parameter that can be related to soot reactivity is the so-called carbon complete conversion time (τ). In this work, the ~~tau~~ τ values have been calculated using the Shrinking Core Model (SCM) equations with decreasing particle size and chemical reaction control conditions [19]. It implies the fitting of the experimental data to the equation Eq. (5), that connects carbon conversion (X_c) and time (t).

$$1 - (1 - X_C)^{1/3} = \frac{t}{\tau} \quad (5)$$

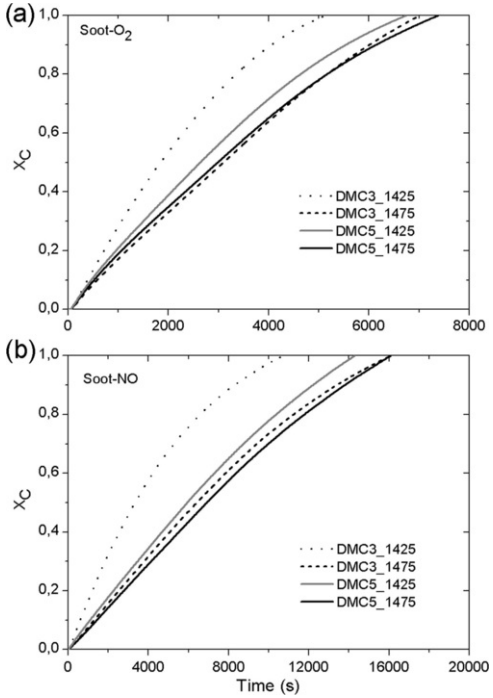

Fig. 6 Evolution of carbon conversion with time for: (a) soot-O_2, and (b) soot-NO interactions.

The τ values obtained for each reactivity experiment are shown in Table 1. A high τ value means that the carbon takes more time to complete its conversion; therefore, the soot samples with high τ value are less reactive than the soot samples with low τ value.

Table 1 Carbon complete conversion time (τ), in seconds, in the soot-O_2 and soot-NO interaction experiments for soot samples obtained with $[DMC]_{inlet}$ = 33,333 and 50,000 ppm at 1425 and 1475 K.

$[DMC]_{inlet}$ (ppm)	1425 K	1475 K

	O_2	NO	O_2	NO
33,333	8979	15,775	14,826	28,318
50,000	12,326	27,524	14,856	33,391

Soot samples DMC3_1475, DMC5_1425, and DMC5_1475 were also characterized using different techniques. Table 2 lists the results of the elemental analysis showing that the principal component of the soot samples is carbon (approximately 98 wt%), with a low content of hydrogen (<0.50 wt%). A more detailed analysis is made with the atomic ratio of carbon to hydrogen (C/H ratio). This is a good measure to assess soot maturity because the soot particles attain a higher degree of carbonization, along with dehydrogenation, throughout their growth [20]. Thus, as the C/H ratio value increases, the soot maturity should increase, and the reactivity decreases. The soot with the highest C/H ratio is that obtained with the highest DMC concentration and at the highest temperature, soot that also presents the lowest reactivity (Table 1).

Table 2 Elemental analysis, C/H ratio, BET surface area, external surface area, and particle size.

Sample	C (wt%)	H (wt%)	C/H (molar basis)	S_{BET} (m^2/g)	S_{EXT} (m^2/g)	d_p (nm)
DMC3_1475	97.92	0.37	21.99	27.27	24.28	99–144
DMC5_1425	97.91	0.45	18.14	32.88	25.33	100–188
DMC5_1475	98.54	0.34	23.80	19.00	16.35	111–188

Table 2 also reports the BET surface area (S_{BET}) values, as well as the external surface area (S_{EXT}). The soot samples have a very low surface area, and show a nonporous character due to the similarity between both areas, S_{BET} and S_{EXT}. This is in agreement with previous works addressing the limited porosity of soot [21]. As the surface area increases, reactivity increases. Thus, surface area values obtained also support what is observed in the reactivity experiments.

To analyze the macroscopic structure of soot, SEM images for three soot samples characterized are presented in Fig. 7. The images show the typical spherule shape of soot particles, as well as the soot particle agglomerates. It is observed that increasing both the soot formation temperature (Fig. 7b and c) and the inlet DMC concentration (Fig. 7a and c), particle size increases and the number of particles decreases, showing a higher surface growth and coagulation effects for the DMC5_1475 soot sample. This supports the elemental analysis results which reveal that the soot sample with a greater maturity is DMC5_1475.

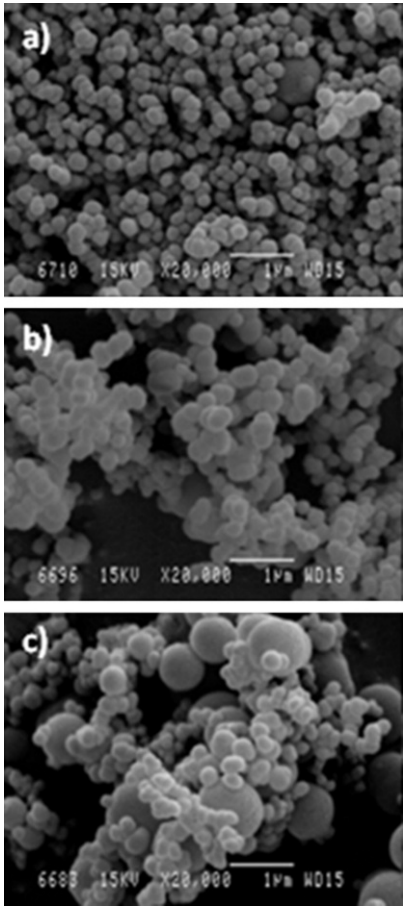

Fig. 7 SEM ~~imagens~~images of soot samples: (a) DMC3_1475, (b) DMC5_1425, and (c) DMC5_1475.

The microscopic structure of soot is studied by TEM. Fig. 8 shows an example of TEM images (DMC3_1475). Similar images are found for the other two soot samples analyzed (DMC5_1425 and DMC5_1475). It is possible to observe the typical chain-like agglomerates (secondary particles) (Fig. 8a) which are composed by several tens or hundreds of spherical or nearly-spherical particles (primary particles) that are held together by physical forces and exhibit the typical onion-shell structure of nanocrystalline graphite (Fig. 8b).

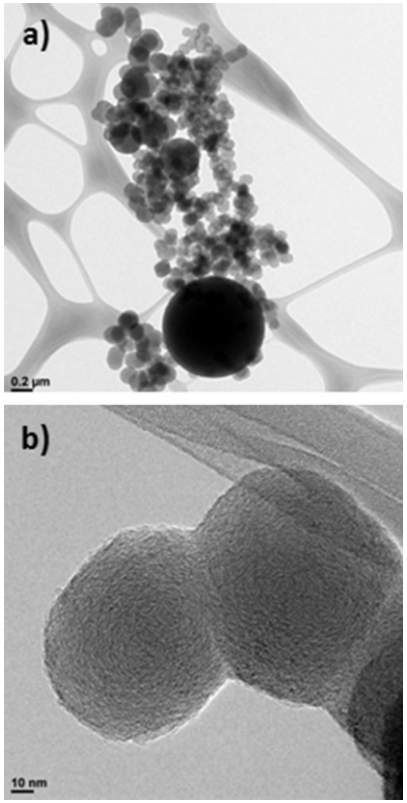

Fig. 8 TEM ~~imagens~~images of soot sample DMC3_1475.

For quantitative information, several TEM images at different resolution were processed to determine the size interval of the particles in each soot sample and the results are listed in Table 2 (d_p). The d_p values (99–188 nm) suggest that the particle sizes are closer to the secondary particle sizes (100–1000 nm) [22].

XRD analysis of soot samples is carried out for evaluating the carbon stacking structure. Fig. 9 shows the X-ray diffractograms obtained. Two characteristic bands are observed: the (0 0 2) band, near 2θ = 24°, which is representative of a crystalline structure, and the (1 0 0) band near 2θ = 44° which indicates the presence of amorphous carbon. The interlayer spacing (d_{002}), the crystallite height (L_c) and diameter (L_a), and the number of layers in a crystallite (k) are calculated using the Bragg's law (Eq. (6)), the Scherrer formula (Eqs. (7) and (8)), and Eq. (9), respectively.

$$d_{002} = \frac{\lambda}{2 \sin \theta_{002}} \quad \textbf{(6)}$$

$$L_c = \frac{K_c \lambda}{B_{002} \cos \theta_{002}} \quad \textbf{(7)}$$

$$L_a = \frac{K_a \lambda}{B_{100} \cos \theta_{100}} \quad \textbf{(8)}$$

$$k = \frac{L_c}{d_{002}} \quad \textbf{(9)}$$

~~Where~~where~~,~~ λ is the wavelength (1.54 Å), θ_{002} and θ_{100} are the Bragg's angles for (0 0 2) and (1 0 0) peaks, respectively, K_c = 0.9, K_a = 1.84, and B_{002} and B_{100} are the FWHM (*full widths at half maximum*) for (0 0 2) and (1 0 0) peaks, respectively. The (0 0 2) and (1 0 0) peaks are fitted to two Gaussian curves in order to obtain the Bragg's angles and FWHM. The calculated structural parameters are

summarized in Table 3.

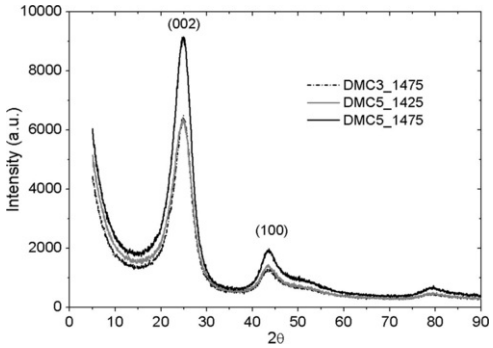

Fig. 9 X-ray diffractograms.

Table 3 Structural parameters extracted from X-ray diffractograms.

Sample	d_{002} (Å)	L_c (Å)	L_a (Å)	k (layers)
DMC3_1475	3.62	18.22	68.60	5.03
DMC5_1425	3.64	16.82	71.38	4.61
DMC5_1475	3.62	18.43	66.26	5.08

For all the soot samples, the interlayer spacing, d_{002}, is higher than that of pure graphite (3.35 Å), suggesting weaker Van der Waals forces of attraction between the crystallites layers and, consequently, a lower order. The slight increase in this value for DMC5_1425 suggests a lower stability of the layers and then a lower order, thus a higher reactivity. It is kwon that the crystallite height, L_c, is directly related to degree of order [23]. The more noticeable decrease in L_c for DMC5_1425 suggests the lowest order, thus the highest reactivity. Due to the low variation of d_{002} and L_c in the soot samples, k (number of layers per crystallite), also shows a negligible variation. L_a value is known to increase with the graphitization degree [24], that is, as L_a increases, reactivity decreases. However, this is not observed in the soot samples analyzed.

Raman spectroscopy is used to determine the degree of graphitization of the soot samples. The Raman spectra of the soot samples are shown in Fig. 10. The main features of these spectra are seen to be two bands; the first one so-called D-band which refers to disordered carbon, and the second one so-called G-band which refers to graphite. The Raman spectra of high-quality graphite crystals only show the G-band, while Raman spectra of defective graphite (when symmetry of the graphene sheets is broken by lattice discontinuities or defects) exhibits the additional D-band. To determine the spectral parameters, i.e., peak position, bandwidth (FWHM), and band intensity, a deconvolution using two Lorentzian lines for D and G bands is carried out. Table 4 summarized these results of fitting.

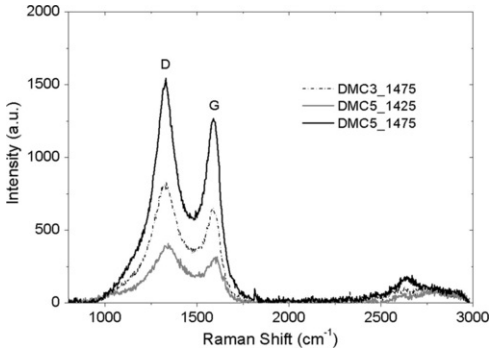

Fig. 10 Raman spectra.

Table 4 Raman spectroscopic parameters obtained from Raman spectra.

Sample	D-band		G-band		I_D/I_G
	Position (cm^{-1})	FWHM (cm^{-1})	Position (cm^{-1})	FWHM (cm^{-1})	
DMC3_1475	1332.2	181.3	1588.5	86.7	1.35
DMC5_1425	1343.9	205.4	1597.6	84.1	1.40
DMC5_1475	1329.8	157.2	1588.9	88.8	1.19

For all the samples, the G-band is narrower that the D-band indicating a low crystallinity of the samples. Moreover, the D-band for DMC5_1475 is narrower than for DMC3_1475, which in turn is narrower than for DMC5_1425. Thus, the soot obtained with the highest DMC concentration and at the highest temperature has the highest degree of order, i.e., is less reactive. This is in accordance with that observed in reactivity experiments and with the other characterization techniques above. The same conclusions can be reached analyzing the intensity ratio I_D/I_G (Table 4), since it is known that the D-band decreases in intensity relative to the G-band with increasing degree of order in the graphite structure.

5 Conclusions

New experimental data on gases and soot formed in the DMC pyrolysis at atmospheric pressure have been obtained. The effect of pyrolysis temperature and inlet DMC concentration on the soot and gas yields has been analyzed. The results demonstrate that both soot and gas yields are affected by the pyrolysis temperature, while an increase in the inlet DMC concentration only affects slightly the soot yield, without notable influence on the gas yield. Experimental data have been complemented with computations based on a gas-phase chemical kinetic model. The model does not include soot particle dynamics, but considers the H-abstraction/C_2H_2-addition (HACA) mechanism and the reaction between resonantly stabilized radicals to describe the PAH formation up to coronene. The model predicts well the gas-phase experimental data trends, though further model development is needed to fit them properly. Results show that DMC has a very low tendency to form soot. The comparison of the amount of soot collected with the sum of the amount of PAH predicted shows that the model can be a good approach toward a complete model including soot formation. Soot reactivity study toward O_2 and NO and its characterization show that the higher the temperature and the inlet DMC concentration of soot formation, the higher the maturity of the soot samples, the lower the surface area, the higher the degree of order, and then the lower the reactivity.

Acknowledgements

The authors express their gratitude to the Aragón Government and European Social Fund (GPT group), and to MINECO and FEDER (Project CTQ2015-65226) for financial support. Ms. K. Alexandrino acknowledges to MINECO for the pre-doctoral Grant awarded (BES-2013-063049).

Appendix A. Supplementary material

Supplementary data associated with this article can be found, in the online version, at http://dx.doi.org/10.1016/j.fuel.2016.06.058.

References

[1] Z.H. Huang, D.M. Jiang, K. Zeng, B. Liu and Z.L. Yang, Combustion characteristics and heat release analysis of a direct injection compression ignition engine fueled with diesel-dimethyl carbonate blends, *Proc Inst Mech Eng, Part D, J Automob Eng* **217**, 2003, 595–606.

[2] P. Rounce, A. Tsolakis, P. Leung and A.P.E. York, A comparison of diesel and biodiesel emissions using dimethyl carbonate as an oxygenated additive, *Energy Fuels* **24**, 2010, 4812–4819.

[3] S.L. Peukert, R. Sivaramakrishnan and J.V. Michael, High temperature shock tube and theoretical studies on the thermal decomposition of dimethyl carbonate and its bimolecular reactions with H and D-atoms, *J Phys Chem A* **117**, 2013, 3718–3728.

[4] A. Sinha and M.J. Thomson, The chemical structures of opposed flow diffusion flames of C3 oxygenated hydrocarbons (isopropanol, dimethoxy methane, and dimethyl carbonate) and their mixtures, *Combust Flame* **136**, 2004, 548–556.

[5] E. Hu, Y. Chen, Z. Zhang, L. Pan, Q. Li, Y. Cheng, et al., Experimental and kinetic study on ignition delay times of dimethyl carbonate at high temperature, *Fuel* **140**, 2015, 626–632.

[6] P.A. Glaude, W.J. Pitz and M.J. Thomson, Chemical kinetic modeling of dimethyl carbonate in an opposed-flow diffusion flame, *Proc Combust Inst* **30**, 2005, 1111–1118.

[7] Alzueta MU, Salinas P, Millera Á, Bilbao R, Abián M. A study of DMC conversion and its impact to minimize soot and NO emissions. 36th Symp. (Int) on Combustion. Seoul, Korea, July 31-August 5, 2016 (accepted for oral presentation). Proc. Combust. Inst. (submitted for publication).

[8] M.P. Ruiz, A. Callejas, Á. Millera, M.U. Alzueta and R. Bilbao, Soot formation from C_2H_2 and C_2H_4 pyrolysis at different temperatures, *J Anal Appl Pyrol* **79**, 2007, 244–251.

[9] C. Esarte, M. Peg, M.P. Ruiz, Á. Millera, R. Bilbao and M.U. Alzueta, Pyrolysis of ethanol: gas and soot products formed, *Ind Eng Chem Res* **50**, 2011, 4412–4419.

[10] K. Alexandrino, Á. Millera, R. Bilbao and M.U. Alzueta, Novel aspects in the pyrolysis and oxidation of 2,5-dimethylfuran, *Proc Combust Inst* **35**, 2015, 1717–1725.

[11] J. Appel, H. Bockhorn and M. Frenklach, Kinetic modeling of soot formation with detailed chemistry and physics: laminar premixed flames of C_2 hydrocarbons, *Combust Flame* **121**, 2000, 122–136.

[12] H. Richter, S. Granata, W.H. Green and J.B. Howard, Detailed modeling of PAH and soot formation in a laminar premixed benzene/oxygen/argon low-pressure flame, *Proc Combust Inst* **30**, 2005, 1397–1405.

[13] M. Frenklach, D.W. Clary, J.W.C. Gardiner and S.E. Stein, Detailed kinetic modeling of soot formation in shock-tube pyrolysis of acetylene, *Proc Combust Inst* **20**, 1985, 887–901.

[14] R.J. Kee, F.M. Rupley and J.A. Miller, Chemkin-II: a Fortran chemical kinetics package for the analysis of gas-phase chemical kinetics, Report SAND87-82151991, Sandia National Laboratories.

[15] K. Alexandrino, P. Salvo, Á. Millera, R. Bilbao and M.U. Alzueta, Influence of the temperature and 2,5-dimethylfuran concentration on its sooting tendency, *Combust Sci Technol* **188**, 2016, 1–16.

[16] M. Abián, Á. Millera, R. Bilbao and M.U. Alzueta, Effect of recirculation gases on soot formation from ethylene pyrolysis, *Combust Sci Technol* **184**, 2012, 980–994.

[17] C. Esarte, Á. Millera, R. Bilbao and M.U. Alzueta, Gas and soot products formed in the pyrolysis of acetylene-ethanol blends under flow reactor conditions, *Fuel Process Technol* **90**, 2009, 496–503.

[18] M.P. Ruiz, R.G. Villoria, Á. Millera, M.U. Alzueta and R. Bilbao, Influence of different operation conditions on soot formation from C_2H_2 pyrolysis, *Ind Eng Chem Res* **46**, 2007, 7550–7560.

[19] O. Levenspiel, Chemical reaction engineering, 3rd ed., 1999, Wiley; New York, 393–440.

[20] Y. Jung and C. Bae, Immaturity of soot particles in exhaust gas for low temperature diesel combustion in a direct injection compression ignition engine, *Fuel* **161**, 2015, 312–322.

[21] H. Burtscher, S. Kunzel and C. Huglin, Characterization of particles in combustion engine exhaust, *J Aerosol Sci* **29**, 1998, 389–396.

[22] B.R. Stanmore, J.F. Brilhac and P. Gilot, The oxidation of soot: a review of experiments, mechanism and models, *Carbon* **39**, 2001, 2247–2268.

[23] R. Hussain and D. Mohammad, X-ray crystallinity studies of palladium polyacrylate, *J Mater Sci Technol* **11**, 1995, 310–312.

[24] K. Al-Qurashi and A.L. Boehman, Impact of exhaust gas recirculation (EGR) on the oxidative reactivity of diesel engine soot, *Combust Flame* **155**, 2008, 675–695.

Appendix A. Supplementary material

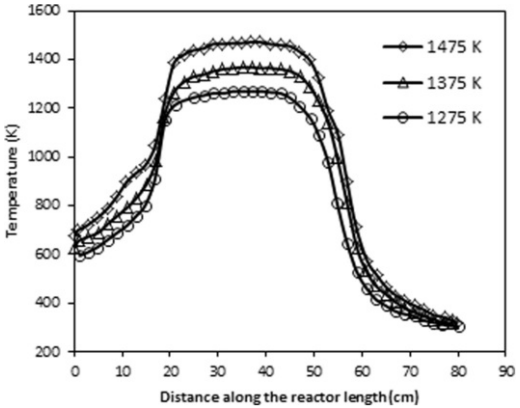

Supplementary Fig. S1 Temperature profiles along the reactor length for 1275, 1375, and 1475 K.

Multimedia Component 1

Supplementary data 1 Mech_DMC.mec file: chemical reaction mechanism.

Multimedia Component 2

Supplementary data 2 Thermdat file: thermodynamic data.

Queries and Answers

Query: Your article is registered as a regular item and is being processed for inclusion in a regular issue of the journal. If this is NOT correct and your article belongs to a Special Issue/Collection please contact aravind.kumar@elsevier.com immediately prior to returning your corrections.
Answer: This is correct

Query: The author names have been tagged as given names and surnames (surnames are highlighted in teal color). Please confirm if they have been identified correctly.
Answer: The author names have been identified correctly

Query: Please check the edits made in affiliations, and correct if necessary.
Answer: Affiliation is correct

Query: One or more sponsor names may have been edited to a standard format that enables better searching and identification of your article. Please check and correct if necessary.
Answer: Sponsor names are correct

Query: Please check the supplementary captions has been set correctly.
Answer: Supplementary captions has been set correctly

Query: Please update Ref. [7].
Answer: The authors do not have the final decission yet.

Query: The country names of the Grant Sponsors are provided below. Please check and correct if necessary. ‘European Social Fund’ - ‘Belgium’, ‘MINECO’ - ‘Spain’, ‘FEDER’ - ‘Spain’.

Answer: The country names of the Grant Sponsors are correct